JOURNAL OF MATERIALS SCIENCE 27 (1992) 3533–3538

Nucleation kinetics of primary crystallization products in FeSiB metallic glasses

M. A. GIBSON*, G. W. DELAMORE
Department of Materials Engineering, University of Wollongong, Wollongong, NSW 2500, Australia

Three iron-based metallic glasses in the $Fe_{96-x}Si_4B_x$ series were examined after various dynamic and isothermal annealing treatments. The number and type of the primary crystallization products formed in these alloys were determined as functions of time and temperature, and the results compared with theoretical models. It has been found that, for certain alloys, a proportion of the primary α-iron crystals in the structure are nucleated by particles of the metastable Fe_3B phase. The transformation kinetics of these composite crystals are different from those which do not contain an Fe_3B core, suggesting different nucleation mechanisms for the two types of crystal.

1. Introduction

Many metallic glasses possess a wide range of desirable properties as a result of their random atomic structure. The completely amorphous state may not, however, provide the optimum properties for all applications; controlled heat treatment to produce a partially crystalline structure may lead to improved properties in some cases. It has been shown, for example, that in certain FeSiB glasses a small volume fraction – around 5 vol % – of suitable crystallites uniformly distributed within the amorphous matrix improves the magnetic properties of such materials when used in devices designed for high frequency applications [1–5]. Successful exploitation of this effect requires a detailed understanding of the crystallization processes of potentially useful alloys, in particular the influence of annealing temperature on the types of phases that crystallize, their spatial distribution and the kinetics of the nucleation and growth processes involved. The temperature of crystallization of metal–metalloid glasses [6, 7] for example, can have a marked effect on the resulting microstructure by altering the nucleation and growth characteristics of competing phases, just as nucleation temperature in highly-undercooled liquid droplets influences phase selection and solidification microstructure [8].

For eutectic or massive (polymorphic) transformations, quantitative information on crystal size distributions as functions of time and temperature can be readily obtained and interpreted in terms of various nucleation and growth models [9]. However, since primary transformations involve solute redistribution and non-linear growth rates, the analysis of this type of transformation is more complex. In such cases the most direct, although laborious, method of analysis of nucleation kinetics is the counting of crystals in samples heat-treated for various times at each annealing temperature. A comparison of such experimentally determined relationships with those predicted by various theoretical models then allows nucleation mechanisms to be determined.

There are a number of possible nucleation mechanisms that may operate during annealing, which can influence the resulting microstructure by dictating the time dependence of crystal formation. These are illustrated schematically in Fig. 1 [10]. For steady-state homogeneous nucleation, the number of crystals increases linearly with time from the onset of crystallization (curve a). With steady-state heterogeneous nucleation, the number of crystals rises linearly at the start of the transformation but as the active sites for nucleation are exhausted, there is a progressive deviation from linearity until site saturation occurs and no new crystals are formed (curve c). For both homogeneous

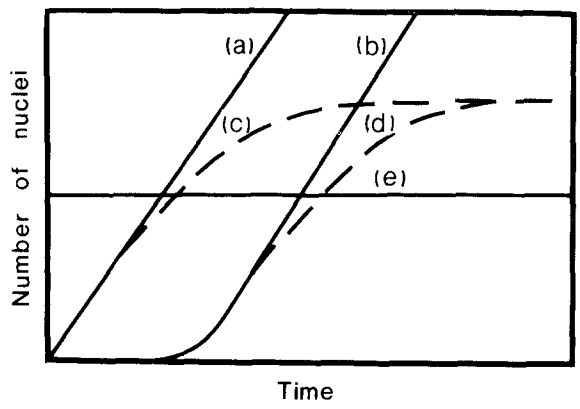

Figure 1 Schematic variation in the number of crystals as a function of isothermal annealing time for different nucleation mechanisms [10]. Nucleation (a) Steady-state homogeneous; (b) transient homogeneous; (c) steady-state heterogeneous; (d) transient heterogeneous; and (e) growth on quenched-in active nuclei.

* *Present address*. CSIRO Division of Materials Science and Technology, Clayton, Victoria 3168, Australia.

and heterogeneous nucleation, initial transient effects may modify the curves to those shown in curves b and d. If crystallization occurs entirely on pre-existing active nuclei, the number of crystals does not change with time throughout the crystallization process (curve e).

The work described here is part of a continuing investigation into the influence of partial crystallization on the magnetic properties of iron-based metallic glasses.

2. Experimental procedure

A series of $Fe_{96-x}Si_4B_x$ alloys was prepared by melting together appropriate amounts of high-purity components in sealed quartz tubes under argon. The resulting alloy buttons were subsequently homogenized by remelting several times on the water-cooled hearth of a small arc furnace, again under argon. Ribbons, approximately 5 mm wide and 25–30 μm thick were melt spun in air using the planar flow casting technique on a stainless steel wheel 300 mm in diameter rotating at 2500 r.p.m.

Differential scanning calorimetry (DSC) was used to characterize the crystallization process and to determine suitable temperatures for isothermal heat treatment. The isothermal annealing experiments were carried out in a lead bath on lengths of ribbon wrapped in aluminium foil and coated in colloidal graphite. Transmission electron microscopy (TEM) was conducted on thinned foils prepared using a Tenupol twin-jet polisher with a solution of 5% perchloric acid in 2-butoxyethanol at 293 K and 60 V.

Crystal numbers were determined from scanning transmission electron micrographs (STEM) taken from specimens annealed for various times at temperatures selected to ensure that primary crystallization products only were produced in the microstructure.

3. Results

3.1. Dynamic heat treatment

A series of dynamic DSC experiments was carried out on the ribbons at heating rates in the range 5–40 K min^{-1}. At each heating rate there is a general trend in the thermogram for a transition from two peaks at low boron concentrations to a single peak at high boron concentrations. In addition, for two of the alloys examined, $Fe_{80}Si_4B_{16}$ and $Fe_{78}Si_4B_{18}$, the shape of the response is dependent on heating rate. As shown in Figs 2 and 3 and in Table I, the ratio of the

TABLE I Ratio of the dynamic peak heights (peak 1/peak 2) for the FeSiB alloys studied as a function of DSC heating rate

Composition (at %)	Heating rate (K min^{-1})			
	5	10	20	40
$Fe_{78}Si_{10}B_{12}$[a]	0.37	0.35	0.33	0.33
$Fe_{82}Si_4B_{14}$	0.24	0.24	0.24	0.26
$Fe_{80}Si_4B_{16}$	0.43	0.59	0.94	1.81
$Fe_{78}Si_4B_{18}$	0.51	0.78	1.57	3.49

[a] Previous unpublished work.

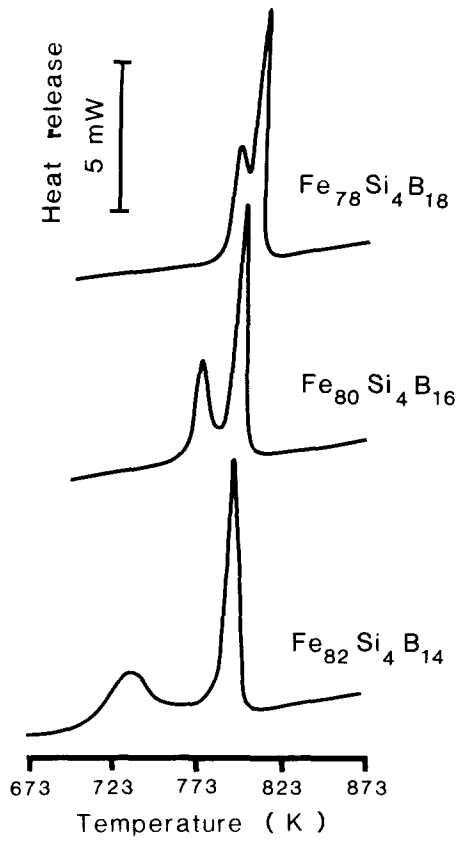

Figure 2 Dynamic DSC scans at 5 K min^{-1}.

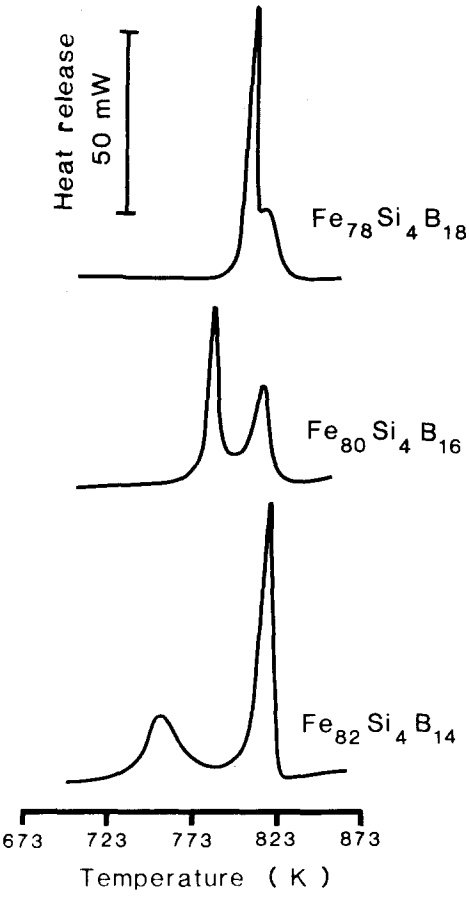

Figure 3 Dynamic DSC scans at 40 K min^{-1}.

heights of the two peaks varies continuously with heating rate for these two alloys, whereas the ratio is essentially independent of heating rate for $Fe_{82}Si_4B_{14}$.

Samples of the various alloy ribbons were also heated to a temperature corresponding to the first peak in the appropriate thermogram and metallographically examined. The primary crystallization product observed in $Fe_{82}Si_4B_{14}$ was dendritic single crystals of α-iron, irrespective of heating rate. The structure of $Fe_{80}Si_4B_{16}$ heated at 5 K min^{-1} is shown in Fig. 4a and consists of a mixture of the single crystal dendrites found in $Fe_{82}Si_4B_{14}$ together with a small amount of a two-phase product consisting of a core of Fe_3B upon which α-iron has nucleated and grown to envelop the Fe_3B, isolating it from the matrix. The layer of α-iron surrounding these composite crystals becomes distinctly dendritic after prolonged periods of growth. At higher heating rates, the proportion of composite crystals in the microstructure increases (Fig. 4b).

A similar primary crystallization sequence was observed for $Fe_{78}Si_4B_{18}$ although the number of composite crystals in the structure was greater at all heating rates than that found in $Fe_{80}Si_4B_{16}$.

3.2. Isothermal heat treatment

3.2.1. $Fe_{82}Si_4B_{14}$

The crystallization sequence in this alloy was known to be a primary reaction followed by a eutectic transformation [11]. At each isothermal annealing temperature selected in these experiments, the only crystallization product observed was the primary reaction product, consisting of single crystal α-iron dendrites. Dynamic DSC scans on the annealed samples showed that only the first peak associated with the transformation had been affected by the isothermal heat treatment and that the second peak, which is associated with the eutectic reaction, was unaltered in size and position.

The α-iron crystals have a distinctly dendritic morphology, even in the very early stages of growth, Fig. 5a. The number of crystals observed as a function of annealing time at each temperature is given in Fig. 6.

3.2.2. $Fe_{80}Si_4B_{16}$

The microstructure of this alloy at the lowest isothermal annealing temperature used, 698 K, consisted entirely of α-iron dendrites as found in $Fe_{82}Si_4B_{14}$. At

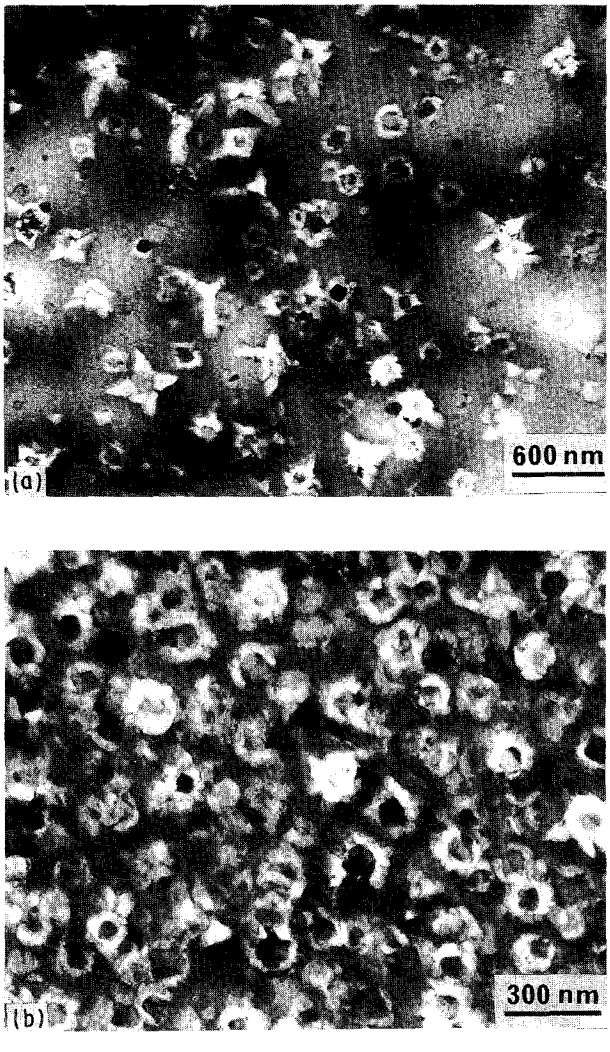

Figure 4 $Fe_{80}Si_4B_{16}$ heated dynamically to a temperature corresponding to the first DSC peak at (a) 5 and (b) 40 K min^{-1}.

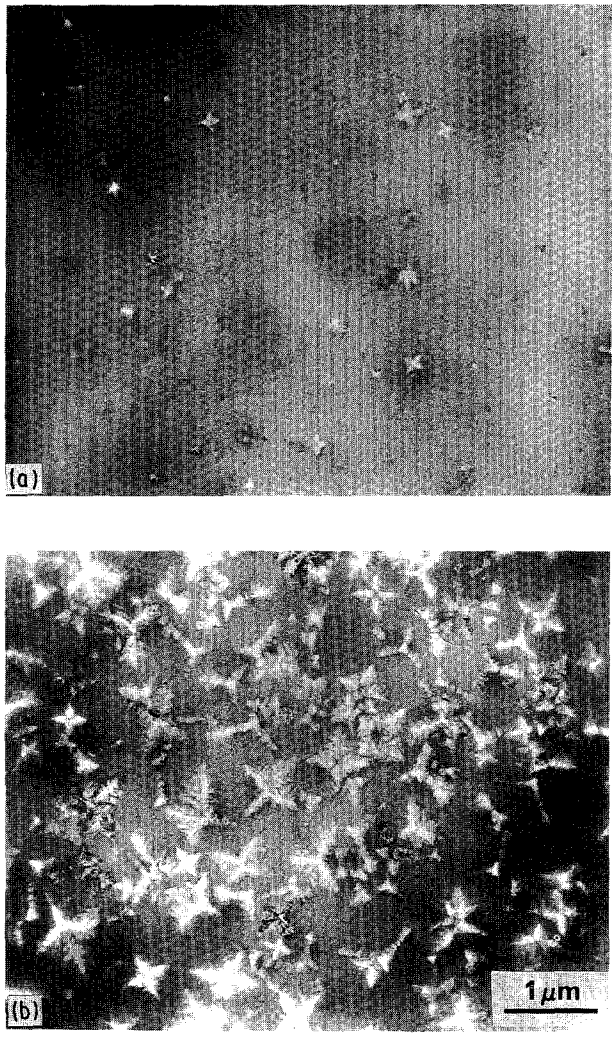

Figure 5 $Fe_{82}Si_4B_{14}$ isothermally annealed at 720 K for (a) 2 and (b) 8 min.

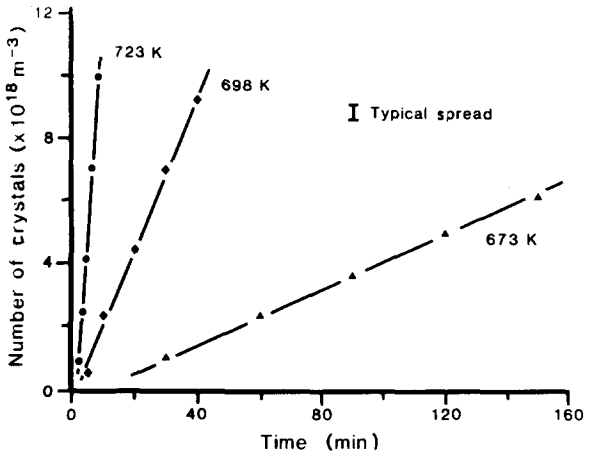

Figure 6 Number of α-iron crystals as functions of time and temperature for $Fe_{82}Si_4B_{14}$.

the higher temperatures, 723 and 748 K, composite crystals identical to those observed under dynamic heating conditions were found in addition to the α-iron dendrites (Fig. 7). The proportion of the composite crystals in the microstructure increased with annealing temperature. The presence of two types of crystallization product in the microstructure added a complication to the process of determination of crystal numbers at large volume fractions transformed as it is difficult to determine whether a given section through a dendrite arm arises from a single crystal or a composite crystal. In general, however, for the earlier stages of the transformation, identification of the two types of crystal was straightforward. The crystal numbers of each product as functions of time at temperature are given in Fig. 8.

3.2.3. $Fe_{78}Si_4B_{18}$

At 723 and 748 K, both types of crystallization product were found in this alloy but at the highest temperature, 773 K, only composite crystals were observed (Fig. 9). Crystal numbers for each type as functions of annealing time and temperature are given in Fig. 10.

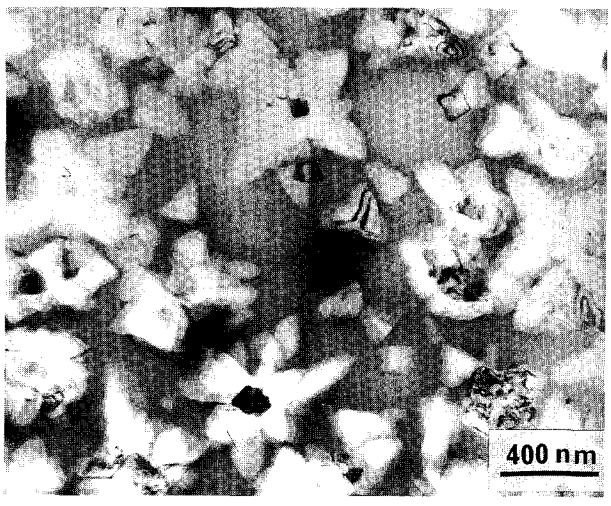

Figure 7 $Fe_{80}Si_4B_{16}$ isothermally annealed at 748 K for 30 min.

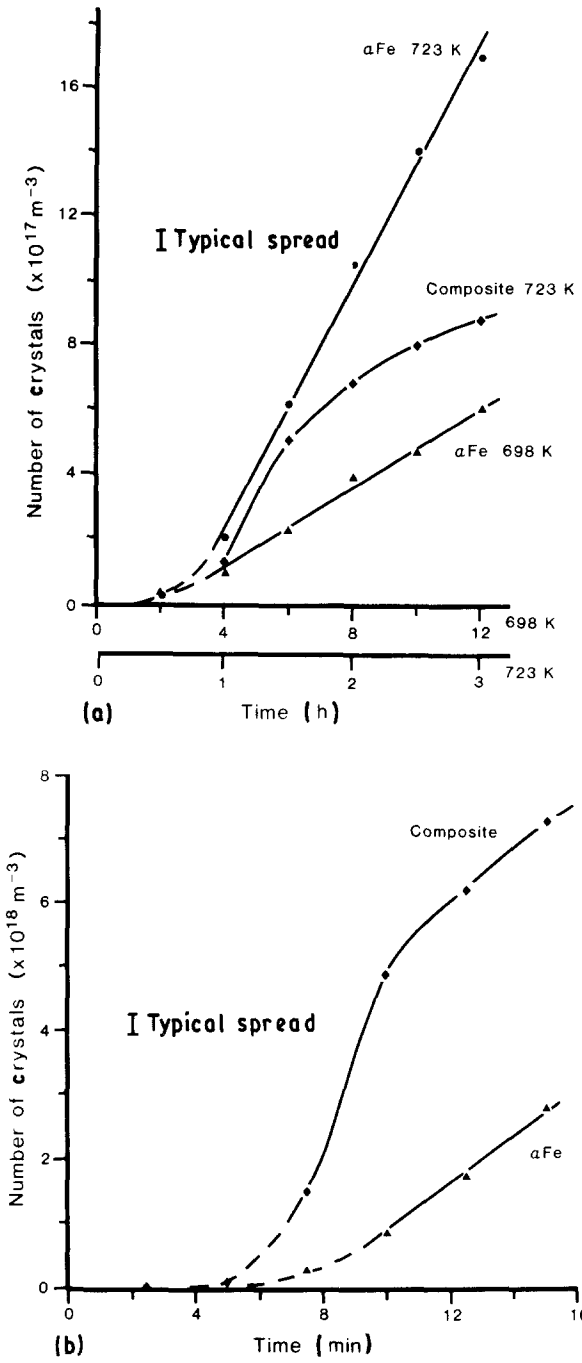

Figure 8 Numbers of α-iron and composite crystals as functions of time and temperature for $Fe_{80}Si_4B_{16}$ annealed at (a) 698 and 723 K; (b) 748 K.

Calculations of nucleation rate and the activation energies for nucleation of the single crystal α-iron dendrites without cores are given in Table II.

4. Discussion

For precise microstructural control by heat treatment, it is important that all factors influencing the crystallization process be considered so that a complete understanding of the transformations involved can be obtained and utilized. DSC is a convenient and sensitive technique for characterizing the crystallization process in metallic glasses, although complementary microstructural observations are usually essential for unambiguous interpretation of the results [12]. If,

TABLE II Crystallization kinetics for α-iron dendrites without Fe_3B cores

Composition (at %)	Nucleation rate (m^{-3})				Activation energy for nucleation ($kJ\,mol^{-1}$)
	673 K	698 K	723 K	748 K	
$Fe_{82}Si_4B_{14}$	6.7×10^{14}	4.1×10^{15}	2.6×10^{16}	–	310
$Fe_{80}Si_4B_{16}$	–	1.8×10^{13}	2.1×10^{14}	3.7×10^{15}	470
$Fe_{78}Si_4B_{18}$	–	–	1.3×10^{14}	6.1×10^{15}	700

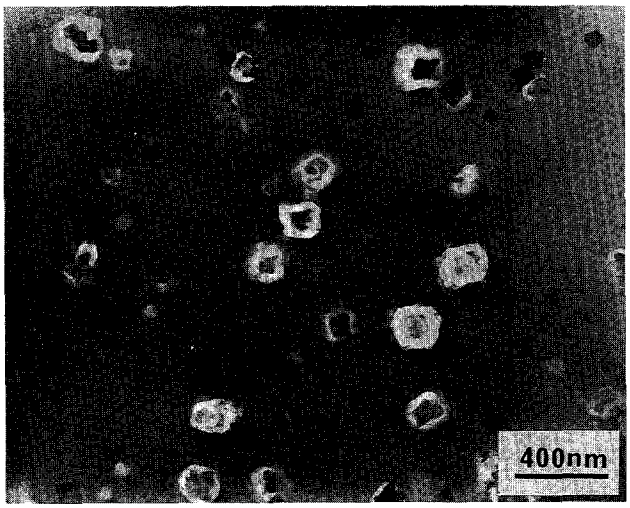

Figure 9 $Fe_{78}Si_4B_{18}$ isothermally annealed at 773 K for 4 min.

however, changes in the dynamic DSC traces result when materials are exposed to different experimental conditions, these changes must arise from differences in crystallization behaviour. The DSC experiments carried out in this investigation showed a systematic variation with heating rate in the shape of the thermogram for both $Fe_{80}Si_4B_{16}$ and $Fe_{78}Si_4B_{18}$ in that the first peak – that associated with primary crystallization – becomes relatively more prominent than the second peak with increasing heating rate. No such variation was found in $Fe_{82}Si_4B_{14}$.

These differences were confirmed by microstructural analysis which showed that at all heating rates (and annealing temperatures in isothermal experiments) only single crystal α-iron dendrites formed during primary crystallization of $Fe_{82}Si_4B_{14}$, as was reported for $Fe_{78}Si_{10}B_{12}$ in a previous study [13]. For $Fe_{80}Si_4B_{16}$ and $Fe_{78}Si_4B_{18}$, the primary crystallization product is a mixture of the α-iron dendrites and a more complex product consisting of a core of Fe_3B surrounded by α-iron, as reported previously for $Fe_{79}Si_5B_{16}$ [14]. The proportion of these complex crystals in the microstructure, as compared with the single-crystal α-iron dendrites, increases with increasing heating rate and is reflected in the increased prominence of the first peak in the dynamic DSC scans. Zaluska and Matya [6, 15] also found that heating rate controlled primary crystallization product selection in FeNiSiB alloys, α-iron dendrites being suppressed in favour of γ-iron at higher heating rates. A similar selection process was found to operate during isothermal annealing at different temperatures, as observed in the present work.

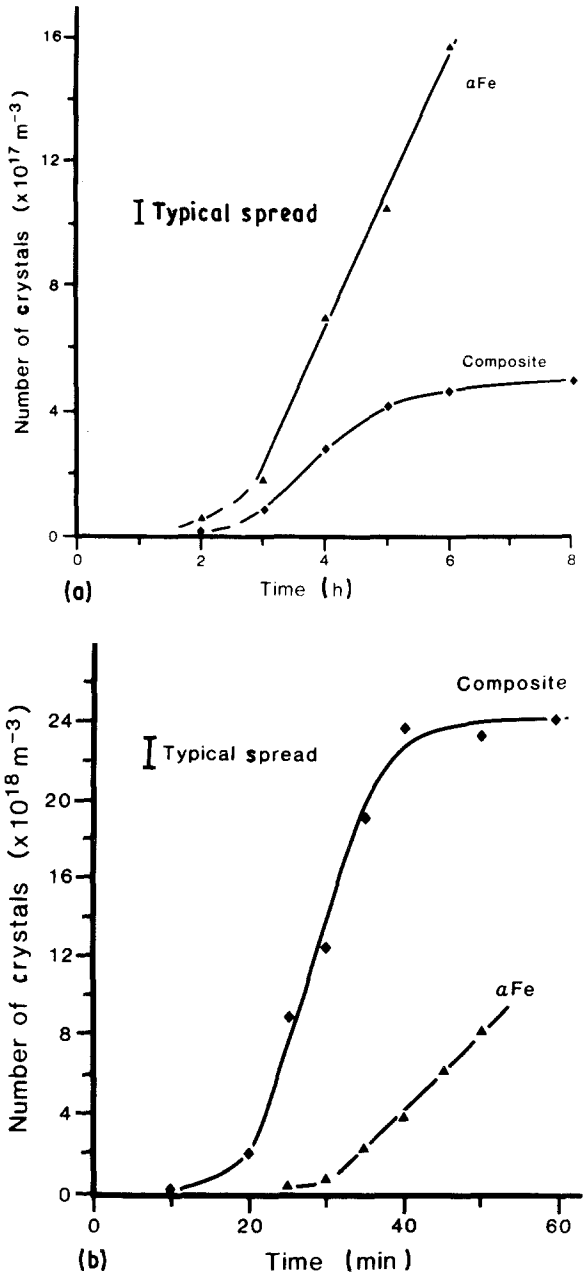

Figure 10 Numbers of α-iron and composite crystals as functions of time and temperature in $Fe_{78}Si_4B_{18}$ annealed at (a) 723 and (b) 748 K.

The transformation kinetics of the two types of primary product are also quite different. The single crystal dendrites show, after some incubation period, a linear increase in crystal numbers with time at each annealing temperature, as shown by the results given in Fig. 6. Comparing these results with the curves in Fig. 1 it is clear that the observed behaviour most

closely resembles that of curve b, i.e. transient homogeneous nucleation. This type of behaviour has been reported previously for primary crystallization products [16].

The nucleation kinetics for the composite crystals match most closely those of curve d in Fig. 1, and are consistent with a thermally activated process occurring at a limited number of quenched-in sites within the matrix. A plausible explanation is that subcritically sized clusters in the melt are retained in the glass during quenching and, during annealing, these clusters reach critical size for growth after some incubation period depending on annealing temperature. Kelton *et al.* [17] have shown that the time required to establish an equilibrium distribution of cluster sizes is restricted during rapid quenching and as a result, the glassy material requires time for growth of sub-critically sized clusters before crystallization can proceed. Although this mechanism is thermally activated, nucleation eventually stops when the quenched-in sites are exhausted. This process is essentially that reported by Greer for $Fe_{80}B_{20}$ alloys [18] and Merk *et al.* [19] for primary crystallization in NiTiB alloys.

Although the sequence of relatively simple structures nucleating on more complex ones is not uncommon during eutectic growth [19], what is unusual in the present work is that the quenched-in clusters first lead to the nucleation and growth of metastable Fe_3B particles which in turn heterogeneously nucleate the stable, primary α-iron phase. Our earlier work [13] showed that the formation of the metastable eutectic of α-iron and Fe_3B in glassy FeSiB alloys is not only restricted to a certain composition range, but is also sensitive to annealing temperature within that range. It seems likely therefore that only certain compositions favour the formation of Fe_3B clusters during quenching, and thence the composite crystals.

Ramanan [5] has reported that optimization of high-frequency magnetic properties by partial crystallization requires control of both precipitate number and size. In addition, the particle crystal structure also influences magnetic properties, the best results being obtained with α-iron crystals: Fe_3B present in eutectic nodules was found to be detrimental to magnetic properties [2]. Whether or not the presence of the Fe_3B core of the composite crystals influences magnetic properties is, however, still to be determined.

5. Conclusions

The type of primary crystals formed during annealing of certain FeSiB metallic glasses in the $Fe_{96-x}Si_4B_x$ series depends on both composition and annealing temperature. In some cases, these crystals nucleate on Fe_3B precursors and the resulting transformation kinetics are significantly different from those without such Fe_3B cores. These results may influence the choice of composition and annealing treatment used to optimize magnetic properties in these alloys.

Acknowledgement

We are grateful for financial support for this work from the Australian Research Council.

References

1. A. DATTA, N. J. CRISTOFARO and L. A. DAVIS, in Proceedings of the Fourth International Conference on Rapidly Quenched Metals, Sendai, 1982, edited by T. Masumoto and K. Susuki (Japan Institute of Metals, Sendai, 1982) p. 1007.
2. R. HASEGAWA, V. R. V. RAMANAN and G. E. FISH, *J. Appl. Phys.* **53** (1982) 2276.
3. D. M. NATHASINGH, *ibid.* **55** (1984) 1793.
4. G. E. FISH and R. HASEGAWA, *ibid.* **63** (1988) 2986.
5. V. R. V. RAMANAN, in "Rapidly Solidified Materials: Properties and Processing", edited by P. W. Lee and J. H. Moll (ASM International, Metals Park, Ohio, 1988) p. 145.
6. A. ZALUSKA and H. MATYJA, *Mater. Sci. Engng.* **97** (1988) 347.
7. M. A. GIBSON and G. W. DELAMORE, *Mater. Sci. Tech.* **4** (1988) 700.
8. R. J. SCHAEFER, L. A. BENDERSKY, D. SHECHTMAN, W. J. BOETTINGER and F. S. BIANCANIELLO, *Metall. Trans.* **17A** (1986) 2117.
9. U. KOSTER and H. BLANKE, *Scripta Metall.* **17** (1983) 495.
10. A. L. GREER, *Mater. Sci. Engng.* **97** (1988) 285.
11. M. A. GIBSON and G. W. DELAMORE, *ibid.* **A117** (1989) 255.
12. *Idem, J. Mater. Sci.* **22** (1987) 4550.
13. *Idem, ibid.* **25** (1990) 93.
14. A. QUIVY, J. RZEPSKI, J. P. CHEVALIER and Y. CALVAYRAC in Proceedings of the Fifth International Conference on Rapidly Quenched Metals, Wurzburg, 1985, edited by S. Steeb and N. Warlimont (Elsevier, Amsterdam, 1985) p. 315.
15. A. ZALUSKA and H. MATYJA, *Int. J. Rapid Solidification* **2** (1986) 205.
16. M. G. SCOTT, G. GREGAN and Y. D. DONG, in Proceedings of the Fourth International Conference on Rapidly Quenched Metals, Sendai, 1982, edited by T. Masumoto and K. Susuki (Japan Institute of Metals, Sendai, 1982) p. 671.
17. K. F. KELTON, A. L. GREER and C. V. THOMPSON, *J. Chem. Phys.* **79** (1983) 6261.
18. A. L. GREER, *Acta Metall.* **30** (1982) 171.
19. N. MERK, D. G. MORRIS and P. STADELMANN, *ibid.* **35** (1987) 2213.

Received 25 February
and accepted 1 September 1991